RSC Advances

ROYAL SOCIETY OF CHEMISTRY

www.rsc.org/advances

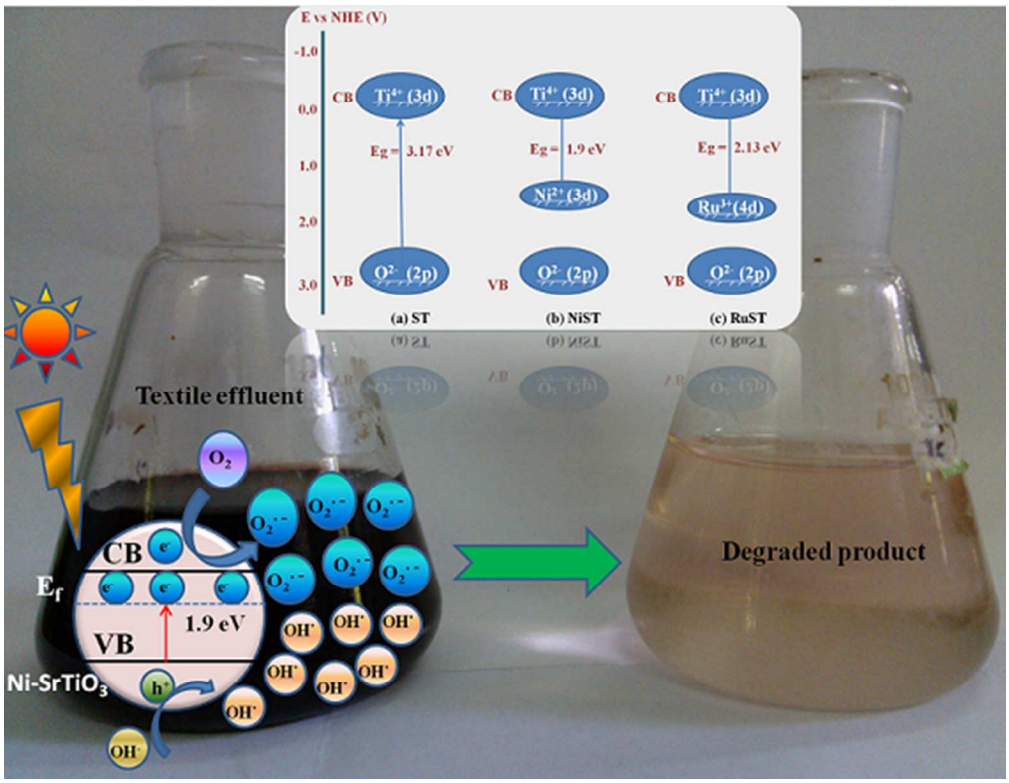

Photomineralisation of textile effluent using highly efficient metal doped titanate catalysts

Metal doped titanate photo catalysts for the mineralization of congored under visible irradiation

Joseph Amala Infant Joice[a] and Thiripuranthagan Sivakumar[a]*

ABSTRACT: *Strontium titanate catalysts and titania were synthesized by sol-gel method. 1 mol % nickel / ruthenium is doped on strontium titanate catalyst to shift its optical response to visible region. UV- Diffuse reflectance spectral analysis confirms the red shift with the band gap of 1.9 eV and 2.13 eV for Ni and Ru doped strontium titanate catalysts respectively. The catalysts were characterized using various instrumental techniques such as X-ray diffraction (XRD), UV- Diffuse reflectance spectroscopy (UV-DRS), Raman spectroscopy, Fourier Transform Infrared spectroscopy (FT-IR), Scanning Electron Microscopy with Energy Dispersive Spectrum (SEM-EDS), Transmission Electron Microscopy (TEM), X-ray photoelectron spectroscopy (XPS). The photocatalytic activities of bare TiO_2, bare strontium titanate and metal impregnated strontium titanate catalysts were evaluated towards the decolourisation / degradation of congored under UV, visible and solar irradiations and monitored by UV-visible spectrophotometer and TOC analyser. Among the catalysts nickel doped strontium titanate completely decolourised CR in the shortest reaction time (300 min) and hence it was subjected to decolourise textile effluent. It was found to be very effective in the degradation of textile effluent as it showed significant reduction in TOC. Kinetic studies imply that the degradation of congored followed pseudo first order kinetics. The recycling test confirmed that the most active nickel doped strontium titanate catalyst is highly photostable.*

---

[a]*Catalysis Laboratory, Dept. of. Applied Science and Technology, A.C.Tech, Anna University, Chennai-25.*

E-mail: tssivakumar@yahoo.com; Tel. : 91-44-22359193

1. Introduction

Dyes from the textile industries pollute the environment due to its intense colour and carcinogenicity has become an issue of a worldwide concern. The release of these dye effluents also cause eutrophication and perturbs to humans and other living organisms. Textile wastewater during printing and dyeing processes is hard to treat due to its higher concentration, deep chromes, great toxicity and complicated component. Azo dyes are the largest group of dyes used for dyeing cotton fabrics in the textile industry.[1-5] By using chemical coagulation method, the azo dyes cannot be removed due to their hydrophilic property. Physico chemical methods such as coagulation and flocculation produce large amounts of sludge which creates disposal problems. Aerobic processes are not suitable to remove azo dyes due to the electron withdrawing nature of the azo bonds.[6-8] Advanced oxidation process has been found to be the most promising technology as it overcomes the limitations of mass transfer, the ability to be carried out at ambient conditions and to completely degrade many organic pollutants including dyes.[9,10] Semiconductors such as TiO_2, ZnO, CeO_2,WO_3, ZnS and CdS are known to be good photocatalysts, among them TiO_2 has been studied widely for the degradation of large number of pollutants such as dyes, phenols, endocrine disruptors and some of these semiconductors were found to be efficient for solar cell applications.[11-19] Apart from these semiconductors, some layered perovskites also have been utilized in the degradation of carcinogens.[20,21] Among layered perovskites $SrTiO_3$ has been used in various fields such as environmental clean-up, hydrogen production and so on due to its excellent dielectric, piezoelectric, and photoelectric properties.[22-28] Recently J. Zhang et al has reported the photo electrochemical applications of these two composite nanotubes.[29] However both TiO_2 and $SrTiO_3$ cannot utilize visible light and make use of only

UV light (> 5%) of the solar beams due to its relatively large bandgap of 3.2 eV.[30] Therefore recent research is devoted to the development of visible-light active photocatalysts. Doping, loading, impregnation and sensitization of strontium titanate catalyst were mainly aimed to shift the light absorption towards the visible light and/or to increase the life time of the electron – hole pairs produced during the photo process.[31-34] One of the present authors has reported the doping/ impregnation of transition metals, noble metals and non- metals into the TiO_2 lattice.[35-37] But the improved photocatalytic activity of transition metal doped $SrTiO_3$ for environmental applications have been rarely reported. J. Zheng et al reported that 94% methylene blue was degraded using Nd doped $SrTiO_3$ nanospheres under visible irradiation.[38] Irie et al reported Pb doped $SrTiO_3$ resulted 0.49 % quantum efficiency towards the decomposition of 2-propanol under visible irradiation.[39] Ag doped $SrTiO_3$ degraded 12% of Victoria blue dye under visible irradiation whereas no activity was observed with Pt and Au doped $SrTiO_3$.[40]

Congored is a water soluble secondary diazo dye. The chemical name of congored is, sodium salt of 3,3'- ([1,1'-biphenyl] -4,4-diyl)bis (4-aminonapthalene-1-sulfonic acid). Benzidine is a toxic metabolite of congo red, which causes cancer of the bladder in humans.[41] Hence studies on the degradation of such harmful pollutant carries significance. Basic chemical information of CR is given in Table ESI1. Lachheb et al have studied the decolourisation of congored using various commercially available titania catalysts.[42] Zhaohong Zhang investigated the degradation of congored using microwave irradiation and attained 87.7% decolourisation using activated carbon powder.[43] Rishi et al have studied the degradation of textile effluent using UV over TiO_2 and obtained 46% degradation within an hour.[44] Li Yun-Cang et al reported the photocatalytic degradation of textile effluent with titania pillar pellets and achieved the degradation of 39%.[45] To the best of our knowledge, no

one has reported the photocatalytic degradation of congored / original textile effluent using metal doped strontium titanate catalysts.

In this paper we report the syntheses of bare (ST) and metal doped strontium titanate viz nickel strontium titanate (NiST) and ruthenium strontium titanate (RuST) catalysts, their characterization by various instrumental techniques such as XRD, UV-DRS, Raman, FT-IR, SEM with EDX, TEM and XPS and evaluated their photocatalytic activities towards the decolourisation / degradation of congored under UV, Visible and sunlight irradiations. The best catalyst among them was chosen and tested for the degradation of original textile effluent collected from a textile industry. The extent of degradation was determined by the Total Organic Carbon analyser and the results were discussed in detail.

2. Experimental

2.1 Materials

Strontium chloride hexa hydrate, citric acid and acetic acid from Sisco Research Laboratories Pvt. Ltd, India, Titanium(IV) iso propoxide from Spectrochem Pvt.Ltd., India, nickel nitrate, congored from Central Drug House, Delhi, ruthenium trichloride from Aldrich were procured and used as such.

2.2 Synthesis of nano titania

Sol- gel process was adopted for the synthesis of titania. 34 mL of TIP and 80 mL of isopropanol were mixed to get solution A. Solution B was prepared by mixing 120 mL of isopropanol, 30 mL of glacial acetic acid and 10 mL of H_2O. Then solution A was mixed to solution B and stirred overnight. The sol obtained was aged to get TiO_2 gel. The gel was dried at 500° C for 3 h and ground to get fine powders of TiO_2.[46]

2.3 Synthesis of strontium titanate and metal doped strontium titanate

30 mL of stoichiometric amount of Sr is added to the solution containing 18.56 mL of TIP and 30 mL of glacial acetic acid and its pH was adjusted to 1.5 with 4M citric acid. The resulting solution was stirred overnight, heated at 65° C for 5 h in waterbath, dried at 110°C for 12 h and again at 180° C for 12 h. Then it was ground, calcined at 400° C for 12 h and again at 650° C for another 12 h to get strontium titanate. NiST and RuST were synthesized by following the above procedure but by adding aqueous solutions of nickel nitrate and ruthenium chloride to the precursors of Sr and Ti to obtain 1 mol% of either Ni or Ru in $SrTiO_3$.[47]

2.4 Characterisation

Rigaku X-ray diffractometer with Cu kα radiation (1.54 nm) was used to find out the phase and composition of the synthesized photocatalysts. The patterns were recorded over a 2θ range of 10-70°. The bandgap measurements of the sample were carried out using Jasco U - 650 Diffuse reflectance spectrophotometer with an integrated sphere using barium sulphate as the reference. FT-IR spectra of all the catalysts were recorded in the range of 4000-400 cm^{-1} using alkali halide technique in a FT-IR spectrometer (Bruker Tensor- 27). Raman measurements were performed at room temperature using Laser Raman Microscope RAMAN – 11. Morphology was studied using scanning electron microscope and the elements present in it was found out using HRSEM-EDAX [Quanta 200 FEG]. High resolution TEM images were obtained with a JEOL JEM 2000EX2 microscope operated at 200 kV. For HRTEM analysis powder samples were sonicated in ethanol for 15 minutes and a drop of it was placed on copper grid and the images were recorded. X-ray photoelectron spectroscopy (XPS)

measurements were performed to find out the elements present in the catalyst on an ECALAB MKIV XPS system with the Al Kα source (1486.6 eV) and a charge neutralizer.

2.5 Photodegradation studies

2.5.1 Photodecolourisation studies of CR using UV- visible spectrophotometer. UV photocatalytic experiments were carried out in a 100 mL quartz vessel containing CR dye solution ($2.5x10^{-4}$M, pH:7.3) and 0.25 g of photocatalyst. Air was purged into the reaction vessel throughout the reaction for proper mixing of the catalyst with the dye solution. Four numbers of mercury lamp (8 W) were used as UV light source. Before illumination the solution was stirred for 30 min in the dark to attain adsorption – desorption equilibrium between the organic substrate and the photocatalyst. Reaction was carried out for 6 ½ h. Visible irradiation experiments were conducted in the same vessel containing the dye solution ($2.5x10^{-5}$ M) using a 500 W, 420 nm visible lamp (Philips). Water was circulated to maintain the room temperature as well as to protect the dye solution from evaporating due to high temperature generated during the reaction. Sunlight irradiation was performed during the summer (month of April) between 10:00 am and 1:00 pm. Solar irradiation experiments were carried out in a glass beaker (100 mL) placed on a magnetic stirrer. Original textile effluent was collected from an industry in Erode District, TamilNadu, India. After filtration the effluent was subjected to photocatalytic decolourisation. Aliquots were withdrawn from the photoreactor at regular intervals. The suspended catalyst particles were centrifuged, filtered through a 0.20 mm filter (Millipore) to remove the fine catalyst particles and the decolourisation was monitored by UV-visible spectrophotometer (HITACHI, U-2000). The absorbance values at the λ max (λ max = 497 nm) of CR were recorded to find out the concentration of dye at different intervals of time. Then the decolourisation of CR was found out using the formula (Eq. 1.),

% decolourisation of CR = $((C_0-C_f)/C_0)*100$ (Eq. 1.)

Whereas C_0 and C_f are the initial and final concentration of CR

2.5.2 Photo mineralisation studies of CR using HPLC and TOC analyser. To find out whether any intermediates have been formed during the degradation of the dye, HPLC analysis was carried out using C18 column. Mixture of methanol and water in the ratio of 30:70 was used as mobile phase. Total organic carbon content of the dye sample was analyzed before and after decolourisation using TOC analyser (SHIMADZU TOC - 500). The sample was placed in a boat of TOC analyser and the organic constituents are converted into CO_2. The gas was dried in the perma pure drier and passed through a particle filter to remove any foreign particles. Then the gas was fed into the NDIR detector, where the concentrations of CO_2 of the samples were measured. From the concentration of CO_2, the TOC was deduced.

3. Results and Discussion

3.1 Characterization of synthesized catalysts

3.1.1 X-ray diffraction analysis. The XRD patterns of bare TiO_2, bare $SrTiO_3$, Ni and Ru doped $SrTiO_3$ are given in Fig. 1. Both bare and metal doped titanates showed sharp and intense XRD peaks indicating high degree of crystallinity. All the x-ray diffraction patterns indicate the presence of single oxide cubic (Pm3m) phase. The sharp peaks at 2θ = 25.3°, 48.05°, 37.8° correspond to (1 0 1), (2 0 0) & (0 0 4) planes and 2θ = 32.5°, 46.5°, 57.8°& 40.01° corresponding to (1 1 0), (2 0 0), (2 1 1) & (1 1 1) planes confirm the presence of anatase phase of titania and cubic (Pm3m) phase of strontium titanates respectively. The patterns match with Joint Committee for Powder Diffraction Studies (JCPDS) files available in the literature (JCPDS file No: 21-1272, file No: 35-0734).[48,49] Due to the very low level

doping (> 1 mol %) of Ni/Ru over strontium titanate, separate peaks for their presence was not observed in the XRD patterns of Ni and Ru doped strontium titanate catalysts. The crystallite size of the synthesized catalysts were calculated using Scherrer's formula ,

$$[D = K\lambda/ \beta \cos \theta] \quad \text{(Eq. 2.)}$$

where β is the full width at half-height, K = 0.89 , θ is the diffraction angle and λ is the X-ray wavelength corresponding to the Cu Kα radiation and given in Table. 1.[50]

(Insert Fig. 1. & Table 1.)

3.1.2 UV diffuse reflectance spectroscopy. Fig. 2A. shows the diffuse reflectance spectra of bare and doped catalysts. The band gap of all the catalysts were determined using the formula $E_g = 1240/ \lambda$, where λ is the cut-off wavelength. This cut-off wavelength is calculated by converting the absorbance into reflectance by performing Kubelka-Munk transformation using the following equation,

$$K/M = (1-R)^2 / 2R \Rightarrow F(R) \quad \text{(Eq. 3.)}$$

where K/M is reflectance transformed according to Kubelka -Munk, R is reflectance (%R), F(R) - Kubelka-Munk function

The corresponding K/M spectra are shown in Fig.2 (B- E). The bandgap values were calculated from these spectra and given in Table. 1. The bandgap values of both the doped catalysts were found to be very low and fall in the visible region when compared to their bare counterparts which confirms the optical response of the catalyst in the visible region.[51] The variation in the bandgap between the metal doped and the bare strontium titanates can be explained by understanding the band structures of the synthesized catalysts. The bandgap values (Table. 1) indicate that the bare and metal doped strontium titanates assume the band structures as shown in Scheme. 1. The bare $SrTiO_3$ has a large bandgap between O^{2-} (2p) and

Ti^{4+} (3d) states and hence it cannot be excited easily under visible light irradiation.[52] However the introduction of metal ion into $SrTiO_3$ lattice creates additional donor levels near the valence band due to the 3d orbitals of Ni^{2+} and 4d orbitals of Ru^{3+} and hence the bandgaps of these two metal doped $SrTiO_3$ catalysts showed lower values of 1.9 eV and 2.13 eV. When $SrTiO_3$ was doped with Cr and nitrogen, similar reduction in bandgaps was observed by Wang et al and Miyarchi et al.[53,54] Generally doping of metals alter the oxygen vacancies and may also act as recombination centres due to which there may be a slight loss in the photocatalytic activity.[47]

(Insert Fig. 2.) & (Scheme. 1)

3.1.3 BET Surface area. The surface area values of bare TiO_2, $SrTiO_3$ and Ni/Ru-$SrTiO_3$ catalysts are given in Table.1. Sol-gel method of syntheses of both titania and strontium titanate led to the formation of highly crystalline compounds. However they differ much in their surface area values. The lower surface area (11-19 m^2/g) obtained in the case of $SrTiO_3$ may be due to the high calcination temperature employed during synthesis. Not much difference in the surface area was seen between bare and metal doped strontium titanates.

3.1.4 Raman spectroscopy. Raman Spectroscopy is one of the most sensitive probes to detect the variation of local symmetry for the surface structure. Raman spectroscopic studies over titania catalyst give information about its phase formation (Fig. 3 (A).). Raman scatterings around 144 cm^{-1} ($E_{g\,(1)}$ the strongest), 200 cm^{-1} ($E_{g(2)}$), 399 cm^{-1} ($B_{1g(1)}$), 519 cm^{-1} ($B_{1g(2)}$) and 639 cm^{-1} ($E_{g(3)}$) indicating TiO_2 is in anatase phase and absence of Raman scatterings around 447 cm^{-1}(E_g strong), 612 (A_{1g} strong) further confirms that rutile phase is absent.[55] $SrTiO_3$ has an ideal cubic perovskite structure with the space group Pm3m with the vibration mode of $3F_{1u}+F_{2u}$ (Fig. 3 (B)). Hence the first order Raman modes are forbidden at room temperature. Du et al have reported the activation of first order Raman modes are

possible by strain effects, oxygen vacancies and external conditions.[56] Each of the F_{1u} modes splits into a doubly degenerate E mode and a nondegenerate A_1 mode, while the F_{2u} mode splits into E and B_1 modes. Thus, the vibration modes are $3(A_1 + E) + E + B_1$. The presence of long-range electrostatic forces further splits each of the A_1 and E modes into transverse optical (TO) and longitudinal optical (LO) modes. Luo et al observed the Raman modes at 484, 547 and 797 cm^{-1} and assigned as LO_3, TO_4 and LO_4.[57] We also observed the bands for bare strontium titanate catalyst at 476 cm^{-1}, 549 cm^{-1} and 802 cm^{-1} due to the above mentioned modes. However for the Nickel and ruthenium doped strontium titanate catalysts these modes were obtained around 472, 514 and 740 cm^{-1} respectively.

(Insert Fig. 3 (A) and (B).)

3.1.5 FT-IR spectroscopy. FTIR spectra of bare and metal doped titania and titanate catalysts are shown in Figure ESI1. The strong peaks around 650 cm^{-1} are due to crystal lattice vibrations of Ti-O-Ti within the TiO_6 octahedra in both titania and titanate catalysts, whereas the other peaks appear around 1400-1600cm^{-1} and 3400cm^{-1} are due to bending and stretching vibrations of adsorbed water molecules .[58-61]

3.1.6 Scanning electron microscopy with energy dispersive spectrum. SEM images generally give information about the shape and size and EDS tells about the composition of the synthesized catalysts. SEM images of the catalysts are shown in Fig. 4 (a)-(d) and their respective EDS are shown in Fig. 4(e) - 5 (h). Both bare and metal doped titanate catalysts show particles of different shape and size. However the shape and size of synthesized titania were found to be almost same. All the samples show peaks between 4.5-5keV due to the presence of Ti in them. The presence of Sr in strontium titanate catalysts are confirmed by the peaks between 1.5-2 keV. Nickel and Ruthenium metal ions show peaks in the regions 7.5-8.4 keV and 2.3-2.9 keV respectively.[62-65]

(Insert Fig. 4.)

3.1.7 Transmission electron microscopy. TEM images of titania, strontium titanate, nickel strontium titanate and ruthenium strontium titanate catalysts are shown in Fig. 5 (a) - (f). Sol-gel synthesis of titania yielded particle with mean diameter of 20 nm (Fig. 5 (a)), whereas the TEM images of metal doped strontium titanates show particles with particle size of 5 nm (Fig. 5 (c-f)). Fig. 5 (b) & (d) show the fringe patterns of titania and ST respectively. Inter planar distance (d) were calculated for both titania (1 0 1) and strontium titanate (1 1 0) and were found to be 0.35 and 0.28 nm respectively. The insets in Fig. 5 (b) and (d) show the SAED patterns of these two catalysts which confirm their crystallinity. The TEM images also revealed that the incorporation of Ni and Ru into $SrTiO_3$ lattice has not altered the morphology. Similar observation was made elsewhere.[66,67]

(Insert Fig. 5.)

3.1.8 X-ray photoelectron spectroscopy. The composition of the elements and the oxidation states of them can be confirmed by the XPS spectra. Fig. 6 (a-c) show the overall spectra of Strontium titanate, nickel /ruthenium strontium titanate catalysts and Fig. 6 (d-h) show the individual spectra of the elements present in the synthesized catalysts. The XPS overall spectra indicated the presence of all the components of strontium titanate (Sr, Ti, O) including the carbon from adsorbed gaseous molecules.[68] The binding energies at 458.1, 458.6, 269.1 and 357.6 eV for Ti ($2p_{1/2}$), Ti ($2p_{3/2}$), Sr (2p) and Sr (3s) respectively.[69] The binding energy at 529.6eV is for O^{2-} ions (Sr-O-Ti) of $SrTiO_3$ frame work. The characteristic Sr 3d doublet line located around 132- 134 eV confirms the presence of strontium as Sr^{2+} in strontium titanate catalyst. Ni ($2p_{3/2}$) peak was observed at 855.8 eV which confirms the presence of nickel and it is existed in form of Ni_2O_3.[70] The binding energy located at 280.6eV for the presence of ruthenium in Ru ($3d_{5/2}$).[71]

(Insert Fig. 6.)

3.2 Photocatalytic studies - Optimization of reaction parameters in the decolourisation of CR

The photocatalytic activity of the synthesized titania catalyst was evaluated towards the decolourisation of congored. Studies on effect of initial concentration, effect of catalyst dosage and effect of pH on the decolourisation of congored were conducted to optimize the reaction parameters.

3.2.1 Effect of initial concentration on the % decolourisation of CR. The influence of initial CR concentration on % decolourisation was studied by varying the concentration from $1x10^{-4}$ M to $3x10^{-4}$ M and at constant catalyst weight of 250 mg at the natural pH of CR. The results obtained are shown in Fig. 7(a). It was observed that the %decolourisation increased with increase in concentration of CR upto $2.5x10^{-4}$ M and on further increasing the concentration to $3x10^{-4}$ M, the % decolourisation decreased. The initial increase in the % decolourisation of CR with increase in the concentration may be attributed to the availability of more number of $OH^{\cdot}$ radicals on the catalyst surface than required. But with increase in the concentration of dye further results in more number of dye molecules which outnumber the $OH^{\cdot}$ radicals and hence there is a reduction in the catalytic activity. In addition, the active sites of the catalyst are covered by dye molecules at higher concentration preventing the passage of light from reaching the surface of the catalyst (screening effect).[72] Hence the concentration at which maximum decolourisation occurs has been optimized at $2.5x10^{-4}$ M.

(Insert Fig. 7)

3.2.2 Effect of catalyst weight on % decolourisation of CR. By keeping the initial concentration of dye constant at $2.5x10^{-4}$ M, the photocatalytic experiments were carried out at the natural pH of the dye solution by varying the weight of the catalyst from 50 to 300 mg. The results obtained in the experiment are shown in Fig. 7(b). Congored was decolourised to different extents (78-100%) at the end of 6 ½ h when the catalyst weight was varied from 50 to 300 mg. The % decolourisation of congored increased and reached 100% when the weight of catalyst was 250 mg and on further increasing the weight to 300 mg a slight decrease in the decolourisation (93%) was observed. A large difference from 48-85% in the % decolourisation was observed at 2 ½ h, when the weight of the catalyst was increased from 50 to 250 mg indicating the faster decolourisation of congored at 250 mg. This may be due to the availability of number of active sites and ˙OH radicals formation with higher catalyst loading. But on further increasing in the catalyst weight to 300 mg, the % decolourisation decreased which may be attributed to the increase in the opacity of the suspension leading to poor penetration of light into the solution. Venkatachalam et al also observed similar decrease in the % decolourisation of organic pollutant at higher catalyst loading and attributed to both increased turbidity and deactivation of activated species by collision with ground state species.[73]

3.2.3 Effect of pH on percentage decolourisation. As pH of the dye solution has profound influence on the adsorption, dissociation of the substrate, catalyst surface charge, oxidation potential of the valence band and other physico - chemical properties of the system, the pH of the dye solution was varied from 3-11 and the experiments were conducted by keeping the initial concentration of the dye at $2.5x10^{-4}$M using 250 mg of TiO_2 and the results obtained at 210 min are shown in Fig.7(c). Varying the solution pH from 3-7, the %

decolourisation was increased reaching maximum (85.8%) at pH 7.3 and at higher pH values the % decolourisation decreased. The behaviour of photocatalyst at different pH can be explained on the basis of point of zero charge (pzc). When the pH of the dye solution is less than pH_{pzc} of titania, the surface of titania is enriched with positive charges and when the pH of dye solution is higher than the pH_{pzc} of titania it becomes negatively charged. In this case pH_{pzc} of titania is 6.8 and hence it is positively charged in acidic medium (pH<6.8) and negatively charged in alkaline medium (pH> 7) . Since CR contains two SO_3^- groups it strongly adsorbs on the positively charged photocatalysts in highly acidic conditions due to electrostatic attraction thus preventing light interacting with the catalyst surface and hence about 10% decrease in decolourisation of congored was observed at pH-3. However at higher pH, about 15% decrease in the decolourisation was observed. This may be due to the electrostatic repulsion taking place between the negatively charged catalysts and the [Dye - SO_3] $^-$ ions. In addition the OH^- ions which are responsible for the formation of $OH^\bullet$ radical are also repelled by the negatively charged catalysts. The pH at which the maximum decolourisation of congored was observed in its natural pH (7.3) and hence further experiments are carried out at pH 7.3.[35,74]

3.2.4 HPLC studies on the degradation of CR. HPLC analysis was carried out to examine whether whether any stable intermediates are formed in the photocatalytic degradation of CR over titania catalyst during the photocatalytic reaction. The samples collected upto 390 min have been subjected to HPLC analysis and the chromatograms are shown in Fig. 8(A). From the chromatogram it is implied that congored is eluted around 8 min. The intensity of this peak was maximum for the sample collected at 0^{th} min and it decreased with time on stream. This shows that CR is degraded with time. However the peak around 8 min is not vanished for the sample collected at 390 min where decolourisation was

found to be 100%. This implies that not all the dye molecules decolourised are degraded. This was well supported by TOC analyses for the sample collected at 390 min (only 32% TOC reduction). The absence of new peaks for the samples collected during the reaction indicates that no other stable intermediates are formed.

(Insert Fig. 8.)

3.3 Evaluation of Photocatalytic activities of bare and metal doped strontium titanate catalysts

The photocatalytic activities of ST, NiST and RuST were evaluated towards the decolourisation of congored under optimized conditions using UV irradiation. The experiment results obtained with titanate catalysts are compared with that of titania and shown in Fig. 9(A). All the catalysts decolourise congored completely but at different reaction times. Among the catalysts NiST showed the highest activity as it decolourises CR in the shortest reaction time (5h). Both metal doped strontium titanate catalysts showed better catalytic activity than their bare counterparts and titania catalysts. This shows that doping of metal into the perovskite lattice has significant effect on the photocatalytic activity. The efficiency of the catalyst in terms of complete decolourisation of CR was found to be in the following order:

NiST > RuST > TiO_2 > ST

(Insert Fig. 9)

HPLC analysis of the dye samples collected at the 240 min in the degradation of CR over NiST is shown in Fig. 8 (B). Like titania NiST also did not form any intermediate in the degradation of CR as no new peaks were seen in the chromatogram.

3.3.1 Kinetic studies of strontium titanate catalysts. Kinetic plots were drawn to find the order of the reaction and rate of decolourisation (Fig.9 (B)). The plots reveal that the decolourisation of CR followed pseudo first order kinetics. The rate constant values obtained from the plots also support the earlier observation that NiST is the best of all the catalysts synthesized and found to be in accordance with the efficiency order discussed above (Table. 1).

3.3.2 Photo mineralisation of Congored. Since different catalysts decolourise CR completely at different times, the extents of mineralisation of CR were determined by TOC analyser at their respective time of complete decolourisation and shown in Fig.9(C). Both bare and metal doped strontium titanate catalysts were found to be very effective in the mineralisation of congored. With metal doped strontium titanate showing high degradation efficiency than the bare catalyst. Like decolourisation NiST showed maximum mineralisation of CR (46%) followed by RuST and ST. The % degradation values were found to be lower when compared to % decolourisation indicating that all the CR molecule which are decolourised completely are not mineralised. This shows that photocatalysts break the chromophoric azo groups leading to decolourisation. The fragments so obtained undergo degradation to different extents.

Fig. 10. shows the spectral changes during congored photodegradation by NiST (0.2mg/L) at its natural pH at different reaction times. The absorption spectrum of the CR dye solution showed three characteristic absorption peaks at 240 nm, 338 nm and 497 nm. The main absorption peak at 497nm belongs to the nitrogen to nitrogen double bond (-N=N-) i.e. for azo chromophore (n -π*transition) which is responsible for the red colour of congored. The other two peaks at 240 nm and 338 nm belong to the structure of benzene (π-π* transition) and naphthalene. The absorption peak at 497nm decreased rapidly with increasing reaction time, and disappeared after 300 min indicating that the azo

chromophores were destroyed. The peaks at 240 nm and 338 nm disappeared with time on stream which confirms the destruction of both benzene and naphthalene rings. The decrease in the TOC values also supports this observation. The absence of new peaks in the decolourisation with time on stream support that the fragmented species do not contain any chromophores (Fig. 10).

(Insert Fig. 10.)

3.3.3 Effluent studies. The efficiency of the best catalyst (NiST) has been tested under UV irradiation for the decolourisation of textile effluent collected from an industry (Dyeing and printing unit, Erode, Tamilnadu, India). As Erode (Tamilnadu, India), has large number of dyeing industries located close to the rivers such as Bhavani, Noyyal and Amaravathi, the area has been chosen for collecting the effluent. Waste water was collected from the flow equalization tank. The colour of the effluent was deep red to black. The effluent characteristics are studied. The intense colour of the effluent, TDS and TOC values reveal that the waste water is highly polluted and need treatment before discharge. Hence the photodecolourisation of the effluent (100mL) collected from the industry has been studied under UV irradiation using NiST (500 mg). The visible spectra of the effluent treated up to 510 min is shown in Fig. 11. The broadness of the visible spectra of effluent indicates that it contains large number of unknown species including dyes. However the synthesized catalyst (NiST) showed a positive decolourisation of unknown dyes with time as evidenced by decrease in the absorption values at 560nm and 625 nm. After 510 min, the peaks at 560 and 625 nm were completely disappeared indicating the high activity of NiST towards the decolourisation of such highly concentrated dark effluent. The inset shows the decrease in the colour with time. The sample collected after 510 min, was subjected to effluent analysis. Reduction shown in the TDS from 6990 to 4230 ppm, Turbidity from 250

to 60 NTU and TOC from 2630 to 2177 ppm values of the treated sample indicate the effectiveness of the photocatalyst.

(Insert Fig. 11.)

3.3.4 Decolourisation of CR under solar and visible irradiations. Solar and visible irradiation experiments were carried out under optimized reaction parameters using all the synthesized strontium titanate catalysts and compared with that of titania (Fig. 12A & B). Since the activity under visible irradiation will be less than under sunlight (includes 4% UV) and UV irradiation the initial concentration of dye was reduced to 10 fold in the photocatalytic decolourisation of CR under visible irradiation. Here also metal doped strontium titanate catalysts showed higher catalytic activity than bare $SrTiO_3$ and TiO_2 catalysts. All the synthesized catalysts showed significant activities both under solar and visible irradiations. However, decolourisation of CR took slightly longer time under solar irradiation than under UV- irradiation for all the catalysts. Among the catalysts NiST decolourised congored quickly (5 ½ h) when compared to other catalysts. Similar observation was also noticed under visible irradiation. Although direct comparison could not be made with time taken for complete decolourisation between UV/Solar and visible studies, the results indicate that a large difference in the % decolourisation of CR was observed between metal doped $SrTiO_3$ and bare titanates. Both bare titania and $SrTiO_3$ are known for poor activity in the visible region due to their wide bandgap. But doping of metals such as Ni and Ru into the lattice creates additional donor levels near the valence band thus reducing the bandgap between CB and VB (1.9 eV and 2.13 eV for NiST and RuST respectively). Between the metal doped strontium titanates, nickel doped strontium titanate showed higher catalytic activity than ruthenium doped strontium titanate. Doping of Ni into $SrTiO_3$ lattice replaces partially the Sr ions forming $Ni_xSr_{1-x}TiO_3$ species whereas

doping of Ru results in the formation of $SrRu_xTi_{1-x}O_3$ species. The lower activity of RuST could be explained as follows: Doping of ruthenium takes place at the photo catalytically active titanium sites and thereby reducing the number of active sites of titania distorting the lattice and creating the defects. Such defects may act as recombination centres for the excitons.[47&75-77]

(Insert Fig. 12)

3.3.5 Recyclability of catalysts. Generally in photocatalysis, strong chemisorption of either dye molecules or intermediates or products may result in significant decrease or even complete loss of photocatalytic activity. Hence the most active catalyst (NiST) was subjected to recyclability test for the photodecolourisation of CR. The catalyst was filtered after every cycle, subjected to further decolourisation with fresh solution of CR [$2.5x10^{-4}$M] and the results are shown in Figure ESI2. The results indicate that not much reduction in % decolourisation was observed after recycling the catalyst four times showing high photo stability.

4. Conclusions

The doping of nickel or ruthenium into strontium titanate lattice shifted the optical response to visible region. TEM measurements and EDS spectra confirmed the presence of doped metals. Oxidation states of the elements present in the catalyst were understood by XPS. Among all the catalysts nickel strontium titanate catalyst showed 100% decolourisation towards CR under UV, visible and sunlight irradiations but at different reaction times. The kinetic plots indicated that the decolourisation of CR followed pseudo first order kinetics. TOC results revealed that 46% of the dye has been degraded. The best catalyst tested with the original textile effluent showed a considerable mineralisation.

Acknowledgements

One of the authors Joseph Amala Infant Joice, thank CSIR, New Delhi, India for the award of Senior Research Fellowship.

References

1 K.Yu, S.Yang, C. Liu, H. Chen, H. Li, C. Sun and S.A. Boyd, *Environ. Sci. Technol.,* 2012, **46**, 7318–7326.

2 P. Bansal and D. Sud, *Desalination,* 2011, **267**, 244–249.

3 P.A. Carneiro, R.F. Pupa Nogueira and M.V.B. Zanoni, *Dyes Pigments,* 2007, **74**, 127–132.

4 J. Amala Infant Joice , R. Ramakrishnan, G. Ramya and T. Sivakumar, *Chem. Eng. J.,* 2012, **210**, 385-397.

5 A. Baan, A. Yodeller, D. Liner, N. Kemmerer and A. Ketchup, *Dyes Pigments,* 2003, **58**, 93–98.

6 S. Zhang, X. Liu, M. Wang, B. Pan and H. Yang, *Environ. Sci. Technol. Lett.,* 2014*,* **1** ,167–171.

7 A.V. Rupa, D. Divakar and T. Sivakumar, *Catal. Lett.,* 2009, **132**, 259–267.

8 G.H. Moon, D.H.Kim, H.I. Kim, A.D.Bokare and W. Choi, *Environ. Sci. Technol. Lett.,* 2014, **1**, 185–190.

9 D.D. Dionysiou, A.P. Khodadoust, A. M. Kern, M.T. Suidan, I. Baudin and J.M. Laine, *Appl. Catal. B: Environ.,* 2000, **24**, 139–155.

10 A.V. Rupa, D. Manikandan, D. Divakar, T. Sivakumar, *J. Hazard. Mater.,* 2007, **147**, 906–913.

11 N. Venkatachalam, M. Palanichamy, Banumathi Arabindoo and V. Murugesan, *J. Mol. Catal. A: Chem.,* 2007, **266**, 158–165.

12 G. A. Suganya Josephine and A. Sivasamy, *Environ. Sci. Technol. Lett.,* 2014, **1**, 172−178.

13 Y. Chen, E. Stathatos and D.D. Dionysiou, *Surf. Coat. Technol.,* 2008, **202**, 1944–1950.

14 K. Sayama, H. Hayashi, T. Arai, M. Yanagida, T. Gunji and H. Sugihara, *Appl. Catal., B* 2010, **94** ,150–157.

15 L. Yue and X.M. Zhang, *J. Alloys Compd.,* 2009, **475**, 702–705.

16 X.J. Wang, F.Q. Wan, K. Han, C.X. Chai and K. Jiang, *Mater. Charact.,* 2008, **59**,1765–1770.

17 S.A. Singh and Giridhar Madras, *Sep. Purif. Technol.,* 2013, **105**, 79–89.

18 Z. Liu, Y. Li, C. Liu, J. Ya, W. Zhao, D. Zhao and Li An, ACS Appl. Mater. Interfaces, 2011, **3**, 1721–1725

19 K. Lee and G. Cao, *J. Phys. Chem. B,* 2005, ***109,*** 11880-11885

20 Y. Huang, Y. Wei, S. Cheng, L. Fan, Y. Li, J. Lin and J. Wu, *Sol. Energ. Mat. Sol. C.* 2010, **94**, 761-766.

21 X. Zhou, J. Shi and C. Li, *J. Phys. Chem. C,* 2011, **115**, 8305 -8311.

22 D.R. Modeshia and R.I.Walton, *Chem. Soc. Rev.,* 2010, **39**, 4303–4325.

23 W. Dong, X. Li, J. Yu, W. Guo, B. Li, L. Tan, C. Li, J. Shi and G. Wang, *Mater. Lett.,* 2012, **67**, 131–134.

24 J.C.Yu, L. Zhang, Q. Li, K.W. Kwong, A.W. Xu and J. Lin, *Langmuir,* 2003, **19**, 7673–7675.

25 W. Jiang, X. Gong, Z. Chen, Y. Hu, X. Zhang and X. Gong, *Ultrason. Sonochem.,* 2007, **14**, 208–212.

26 Y. Liu, L. Xie, Y. Li, R. Yanga, J, Qu, Y. Li and X. Li, *Power Sources,* 2008, **183**, 701–707.

27 U. Sulaeman, S. Yin and T. Sato, *Appl. Catal., B*, 2011, **105**, 206–210.

28 K. Guo, Z. Liu, Y, Wang, Y. Zhao, Y. Xiao, J. Han, Y. Li, B. Wang and T. Cui, Int. J.Hydrogen energy , 2014, **39**, 13408-13414.

29 J. Zhang, J.Bang, C.Tang and P.V. Kamat, ACS Nano, 2010, **4**, 387–395

30 H.F. Liu, *Solid State.Commun.,* 2012, **152**, 2063–2065.

31 A. D.Paola, E. G. Lopez, G. Marci and L. Palmisan, *J. Hazard. Mater.,* 2010, **211**, 3–29.

32 J. Wang, S. Yin, Q. Zhang, F. Saito and T. Sato, *J. Mater. Chem.,* 2003, **13**, 2348-2352.

33 Chia- Hao Chang and Yun-Hwei Shen, *Mater. Lett.,* 2006, **60**, 129-132.

34 J. Wang, S. Yin, M. Komatsu and T. Sato, *J. Eur. Ceram. Soc.,* 2005, **25**, 3207-3212.

35 R. Vaithiyanathan and T. Sivakumar, *Water Sci. Technol.,* 2011, **63**, 377–384.

36 R. Ramakrishnan, S. Kalaivani, J. Amala Infant Joice and T. Sivakumar, *Appl. Surf. Sci.,* 2012, **258**, 2515–2521.

37 A.V. Rupa, R. Vaithiyanathan and T. Sivakumar, *Water Sci. Technol.,* 2011, **64**, 1040–1045.

38 J. Zheng, Y. Zhu, J. Xu, B. Lu, C. Qi, F. Chen and J. Wu, *Mater. Lett.,* 2013, **100**, 62–65.

39 H. Irie, Y. Maruyama and K. Hashimoto, *J. Phys, Chem. C,* 2007, **111**, 1847–1852.

40 V. Subramanian, R. K. Roeder and E. E. Wolf, *Ind. Eng. Chem. Res.,* 2006, **45**, 2187–2193.

41 V. A. Sakkas, M. A. Islam, C. Stalikas and T. A. Albanis, *J. Hazard. Mater.,* 2010, **175**, 33–44.

42 H. Lachheb, E. Puzenat, A. Houas, M. Ksibi, E. Elaloui, C. Guillard and J.M. Herrmann, *Appl. Catal. B*, 2002, **39**, 75–90.

43 Z. Zhang, Y. Shan, J. Wang, H. Ling, S. Zhang, W. Gao, Z. Zhao and H. Zhang, *J. Hazard. Mater.,* 2007, **147**, 325–333.

44 Rishi Ananthashankar and Abdel Ghaly, *Am. J. Engg. Appl. Sci.,* 2013, **3**, 252–262.

45 L.Yun-cang, Z. Lin-da and E. Hu, *J. Environ. Sci.,* 2004, **3**, 375–379.

46 E. Sanchenz and T. Lopez, *Mater. Lett.,* 1995, **25**, 271- 275.

47 A. Jia, Z. Su, L.L. Lou and S. Liu, *Solid State Sci.,* 2010, **12**, 1140–1145.

48 I.K. Battisha, A. Speghini, S. Polizzi, F. Agnoli and M. Bettinelli, *Mater. Lett.,* 2002, **57**, 183–187.

49 C.N. George, J.K. Thomas, R. Jose, H. Padmakumar, M.K.Suresh, V. Ratheesh Kumar, P.R. Shobana Wariar and J. Koshy, *J. Alloys Compd.,* 2009, **486**, 711–715.

50 Y. Wu, J. Zhang, L. Xiao and F. Chen, *Appl. Catal. B,* 2009, **88**, 525–532.

51 B.W.Faughnan, Photochromism in Transition-metal-doped $SrTiO_3$, *Phys. Rev. B,* 1971, **4**, 3623-3636.

52 R. Niishiro, H. Kato and A. Kudo, *Phys. Chem. Chem. Phys.,* 2005, **7**, 2241–2245

53 D. Wang, J. Ye, T. Kako and T. Kimura, *J. Phys. Chem. B,* 2006, **110**, 15824-15830.

54 M. Miyauchi, M. Takashio and H. Tobimatsu, Langmuir., 2004, **20**, 232-236.

55 X. Chen and S.S. Mao, *Chem. Rev.,* 2007, **107**, 2891–2959.

56 Y.L. Du, G. Chen and M.S. Zhang, *Solid State Commun.,* 2004, **130**, 577–580.

57 W. Luo, Z. Li, X. Jiang, T. Yu, L. Liu, X. Chen, J. Yead and Z. Zou, *Phys. Chem. Chem. Phys.,* 2008, **10**, 6717–6723.

58 T. Bezrodna, G. Puchkovska, V. Shimanovska and J. Baran, *Mol. Cryst. Liq. Cryst.,* 2004, **13**, 71–80.

59 O. Liang, X. Shen, F.Song, M. Liu, *J. Mater. Sci. Technol.,* 2011, **27**, 996–1000.

60 T. Ohno, T. Tsubota, Y. Nakamura and K. Sayama, *Appl. Catal. A,* 2005, **288**, 74–79.

61 A.Z. Simoes, F. Moura, T.B. Onofre, M.A. Ramirez, J.A. Varela and E. Longo, *J. Alloys. Compd.,* 2010, **508**, 620–624.

62 T.Tsumura, K.Sogabe and M. Toyoda, *Mater. Sci. Eng. B.,* 2009, **157**, 113–115.

63 M.Yousefpour and A. Shokuhy, *Superlattices and Microstructures,* 2012, **51**, 842–853.

64 H.Tseng, M.ChiWei, S.Hsiung and C.Chiou, *Chem. Eng. J.,* 2009, **150**, 160–167.

65 V. Houskova , V. Stengl, S. Bakardjieva, N. Murafa and V. Tyrpekl, *Appl. Catal. B: Environ.,* 2009, **89**,613– 619.

66 D.N. Bui, J. Mu, L. Wang, S.Z. Kang and X. Li, *Appl. Surf. Sci.,* 2013, **274**, 328–333.

67 T. Setinc, M. Spreitzer, D.Vengust, I. Jerman and D. Suvorov, *Ceram. Int.,* 2013, **39**, 6727–6734.

68 H.L. Li, Z.N. Du, G.L. Wang and Y.C. Zhang, *Mater. Lett.,* 2010, **64**, 43–434.

69 B.Huang, E.Su and M.Wey, *Chem. Eng. J.,* 2013, **223**, 854–859.

70 N. S. Mclntyre and M. G. Cook, *Anal. Chem.,* 1975, **47**, 2208-2213.

71 M. A. Khan, D. H. Han and O. Yang, *Appl. Surf. Sci.,* 2009, **255**, 3687–3690.

72 L. Kumaresan, A. Prabhu, M. Planichamy and V. Murugesan, *Mater. Chem. Phys.,* 2011, **126**, 445–452.

73 N. Venkatachalam, M. Palanichamy, Banumathi Arabindoo and V. Murugesan, *J. Mol. Catal. A: Chem.,* 2007, **266**, 158–165.

74 U.G. Akpan and B.H. Hameed, *Chem. Eng. J.,* 2011,**169**, 91–99.

75 A.Kudo, R. Niishiro, A. Iwase and H.Kato, Chem.Phys.,2007, **339** ,104–110

76 H. Li, S. Yin, Y. Wang, T. Sekino, S. W. Lee and T. Sato, J. Catal., 2013, **297,** 65–69

77 T. Ohno, F. Tanigawa, K. Fujihara, S. Izumi and M. Matsumura, J. Photochem. Photobiol. A, 1999, **127**, 107–110

Table

Table. 1. Crystallite size, bandgap, surface area and their rate constant values in the degradation of CR

S.No	Catalysts	Crystallite size (nm)	Bandgap (eV)	BET surface area(m^2/g)	Rate constant (min-1)
1	TiO_2	19	3.17	93	$9.21x10^{-3}$
2	ST	43	3.17	11	$7.13x10^{-3}$
3	NiST	39	1.9	16	$1.26x10^{-2}$
4	RuST	38	2.13	19	$1.08x10^{-2}$

Figures

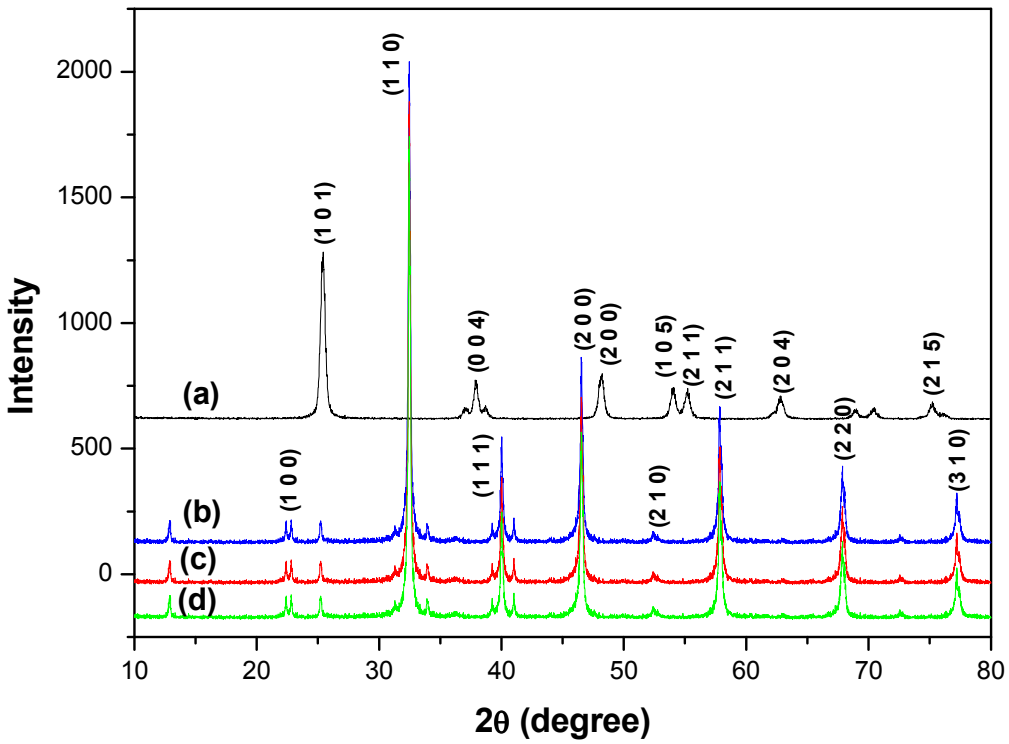

Fig. 1 XRD patterns of (a) bare TiO_2 (b) ST, (c) NiST and d) RuST

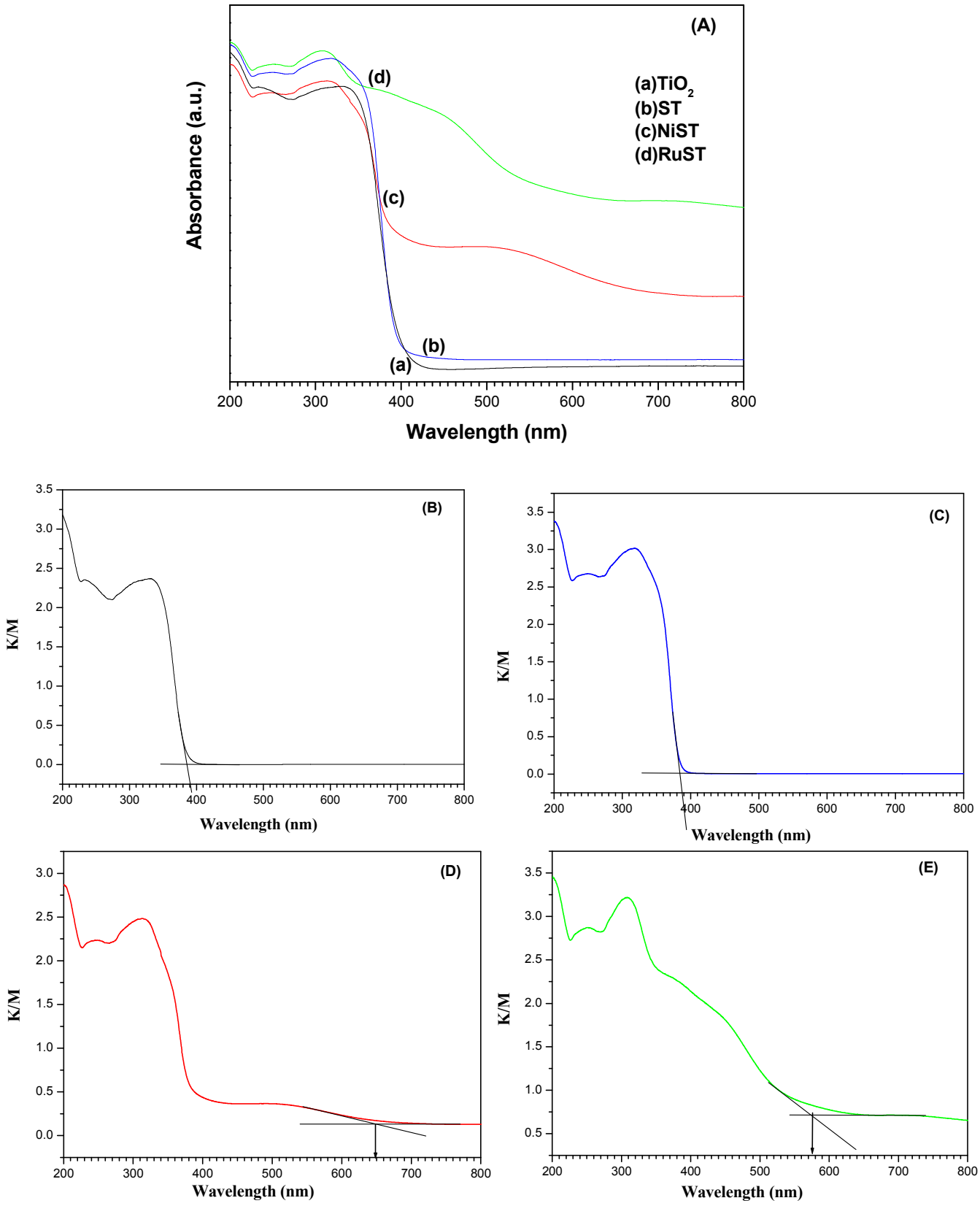

Fig. 2 (A) UV- DRS absorption spectra of (a) bare TiO_2 (b) ST, (c) NiST and (d) RuST. and (B) – (E) their corresponding Kubelka-Munk spectra

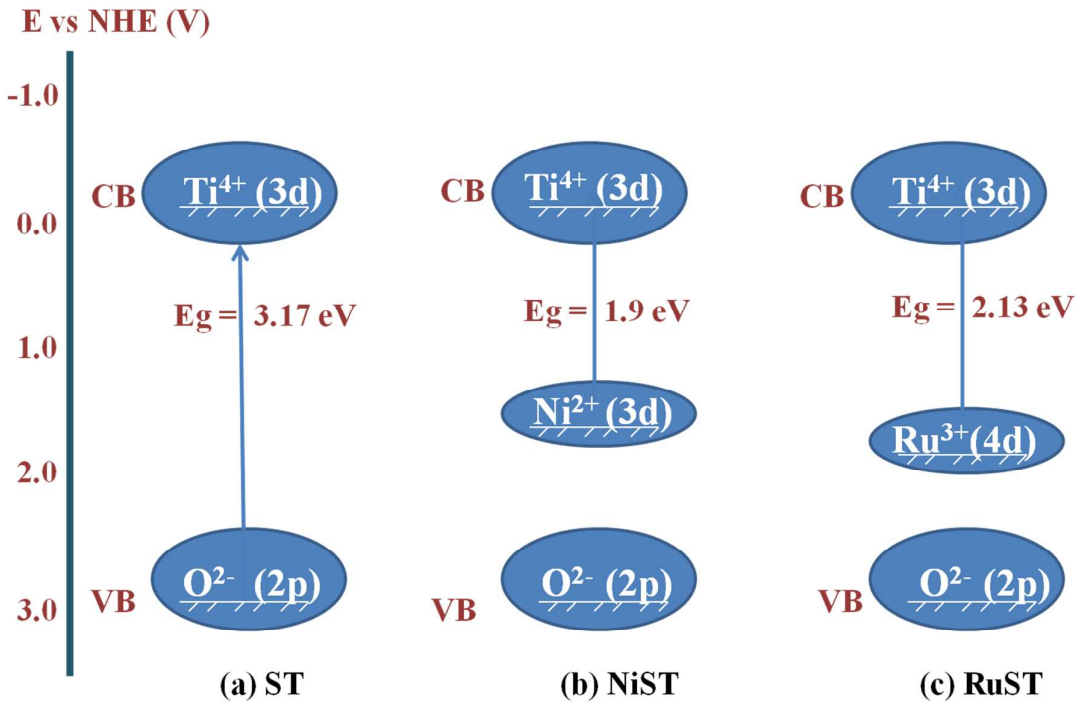

Scheme. 1 Band structures of ST, NiST and RUST

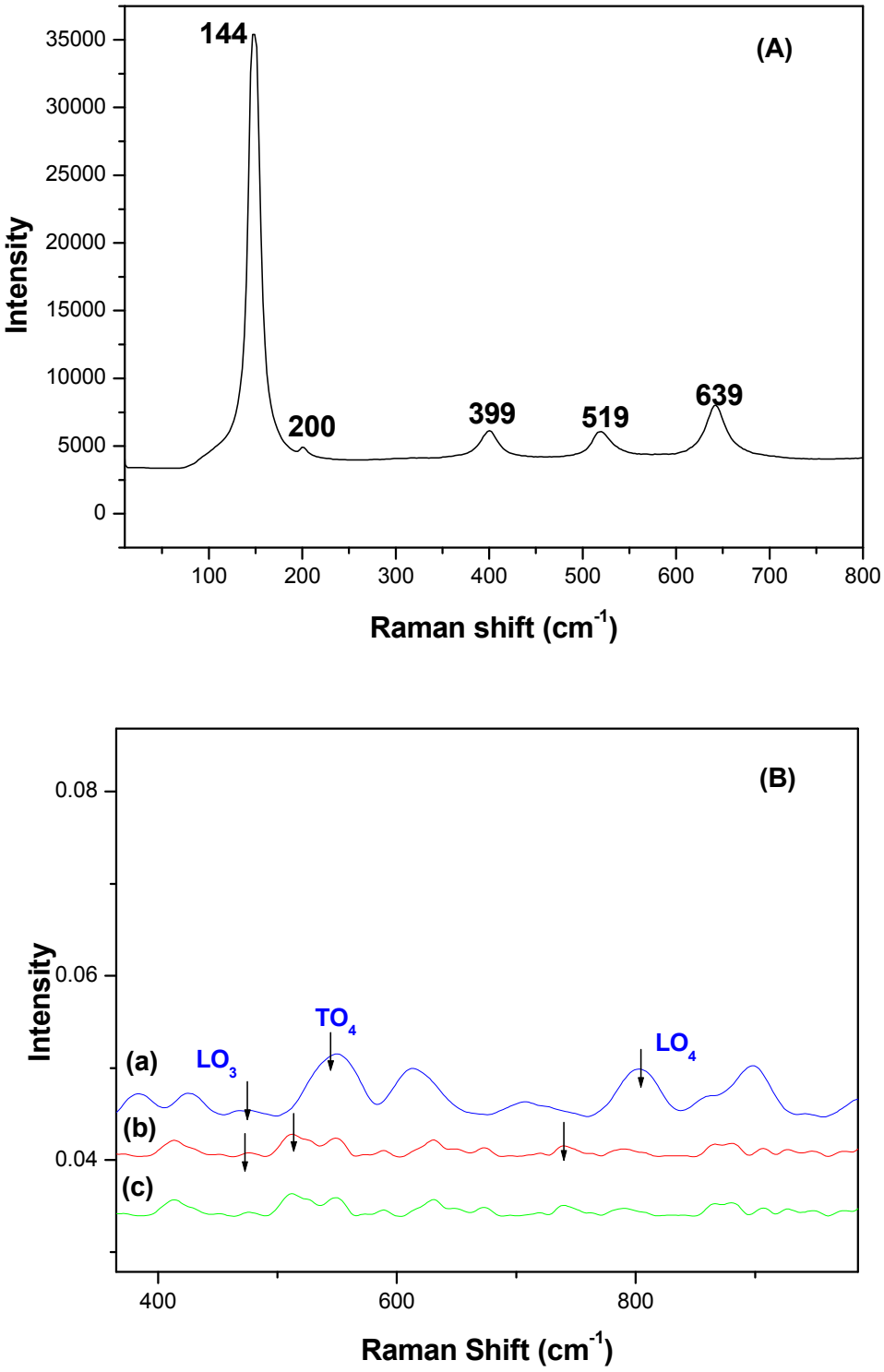

Fig. 3 (A) Raman spectra of bare TiO_2 **(B)** Raman spectra of (a) ST, (b) NiST and (c) RuST

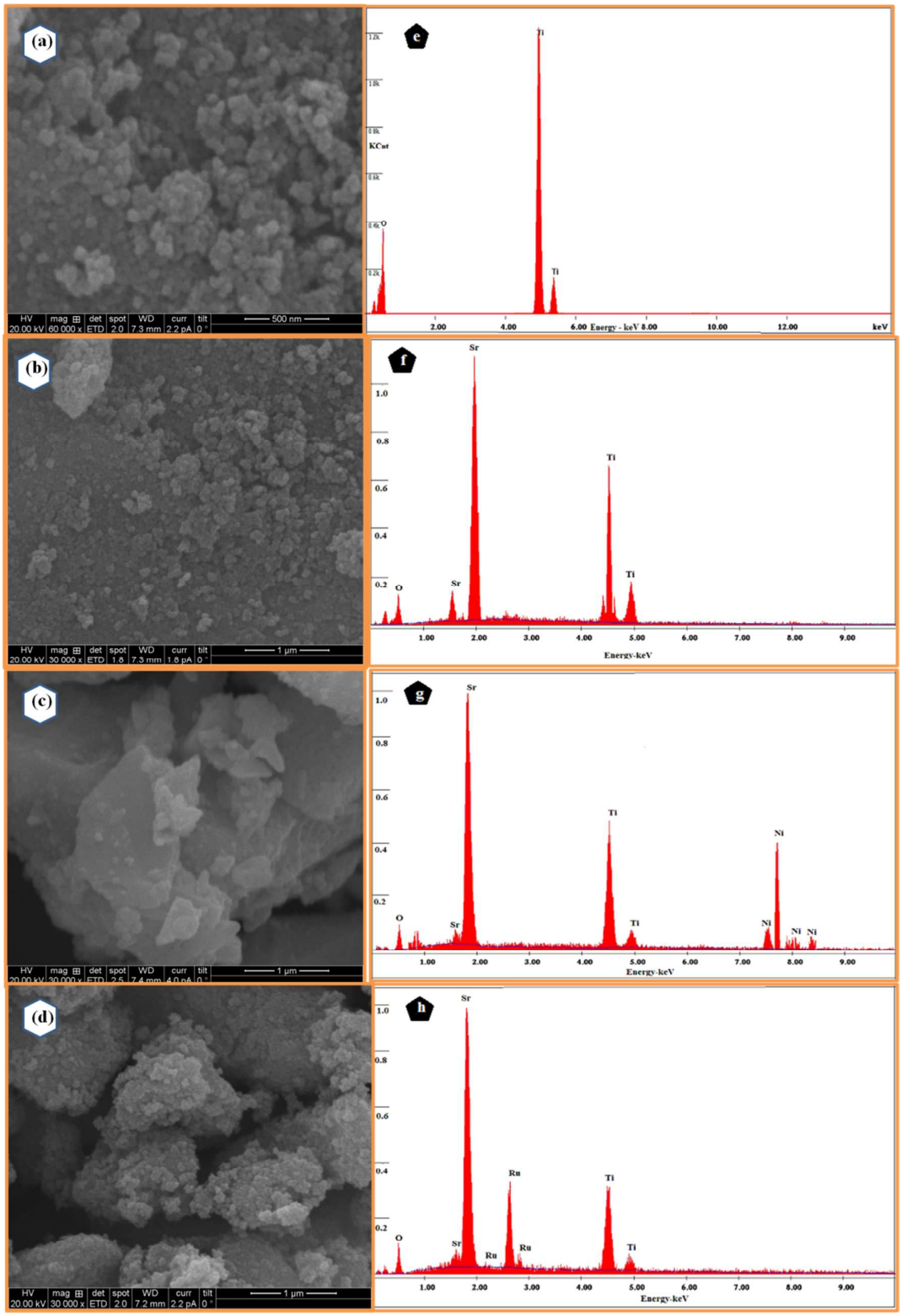

Fig. 4 SEM images of (a) bare TiO_2, (b) ST, (c) NiST and (d) RuST ; EDS spectra of (e) bare TiO_2 , (f) ST, (g) NiST and (h) RuST

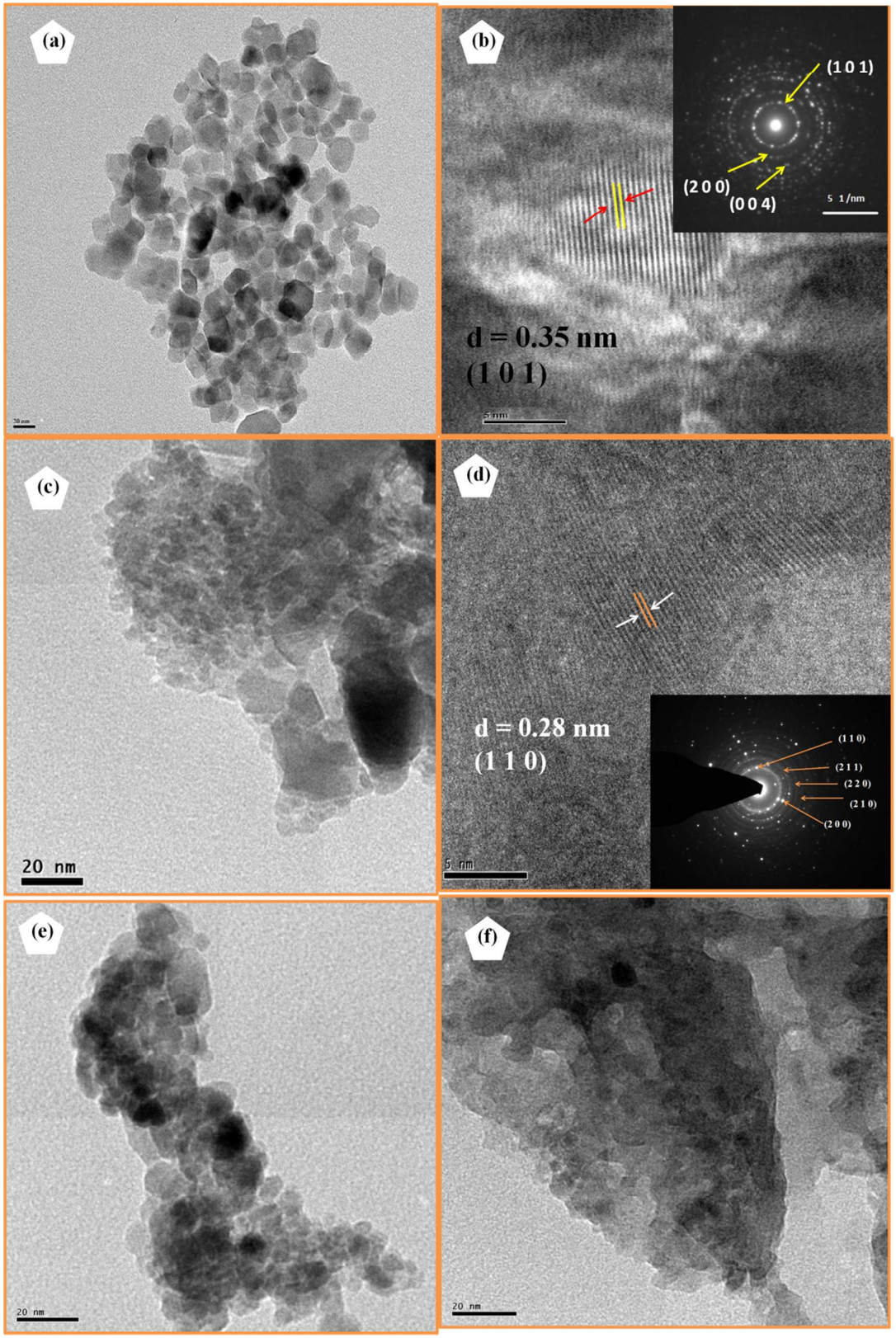

Fig. 5 TEM images of (a) and (b) bare.TiO_2 , (c) and (d) ST, (e) NiST (f) RuST, Insets show their corresponding SAED patterns

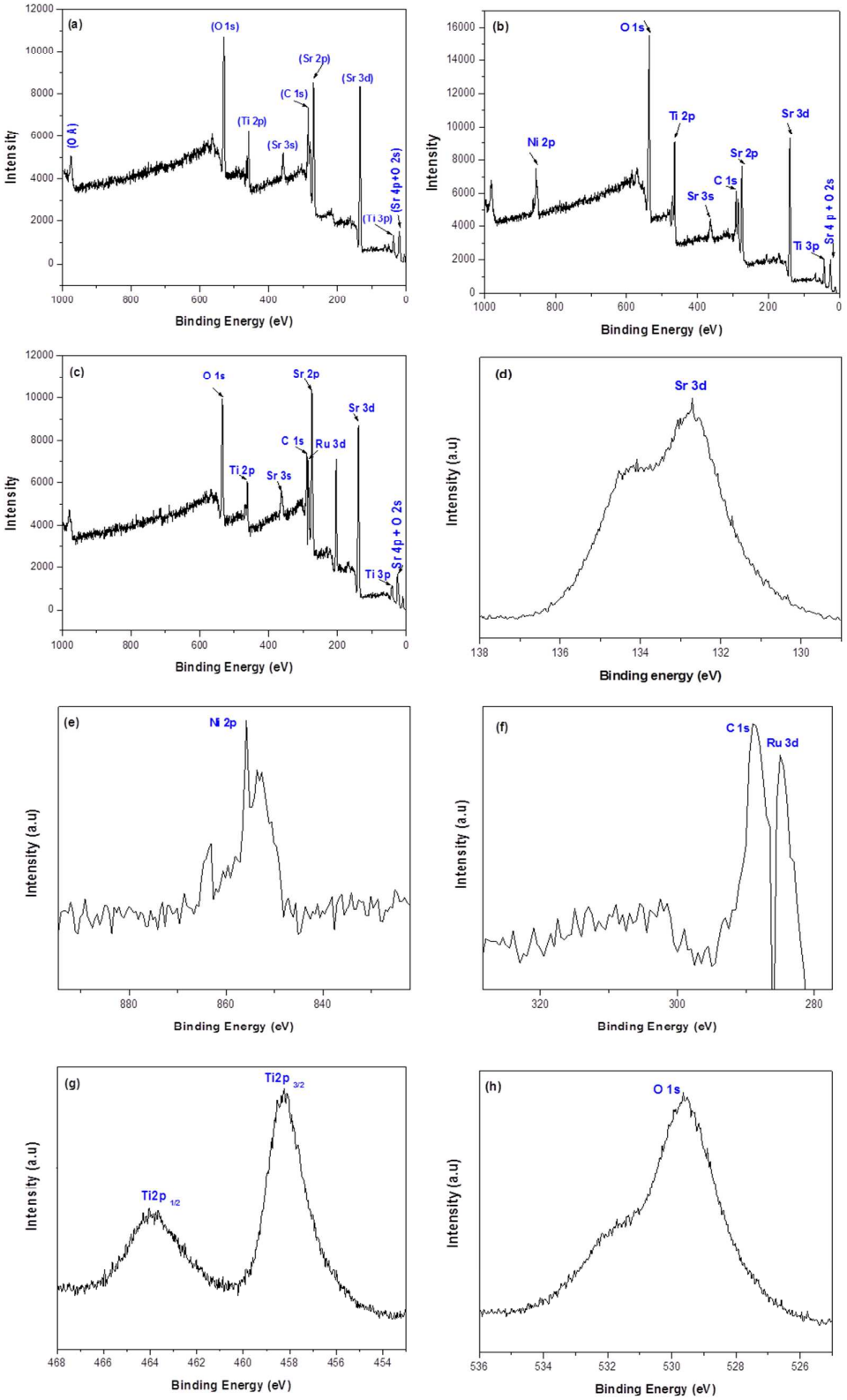

Fig. 6 Overall XPS spectra of (a) ST, (b) NiST , (c) RuST and Individual XPS spectra of (d)-(h) Sr, Ni, Ru, Ti and O

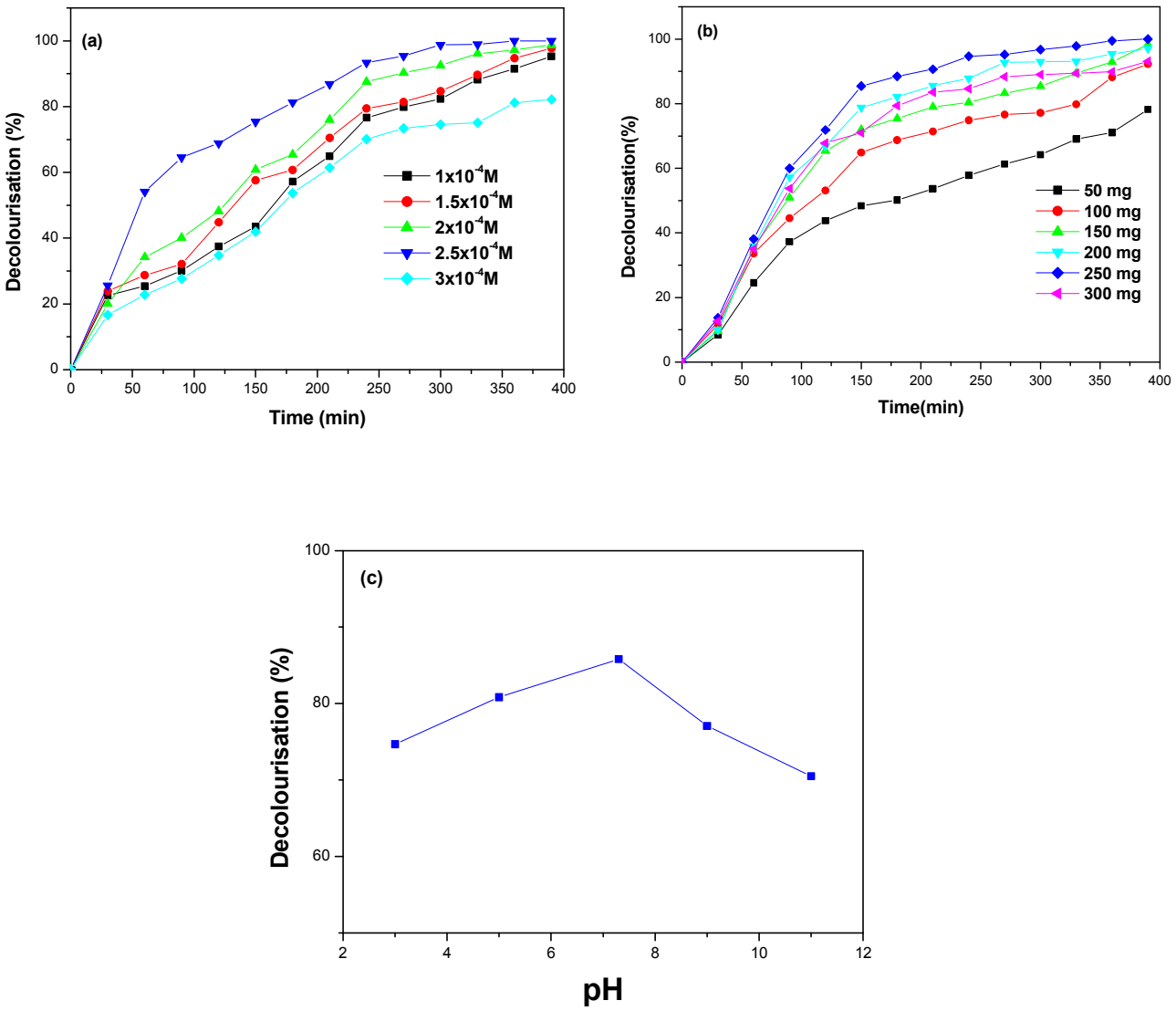

Fig. 7 Effect of (a) Initial concentration of CR (b) catalyst weight (TiO_2) and (c) pH on % decolourisation of CR

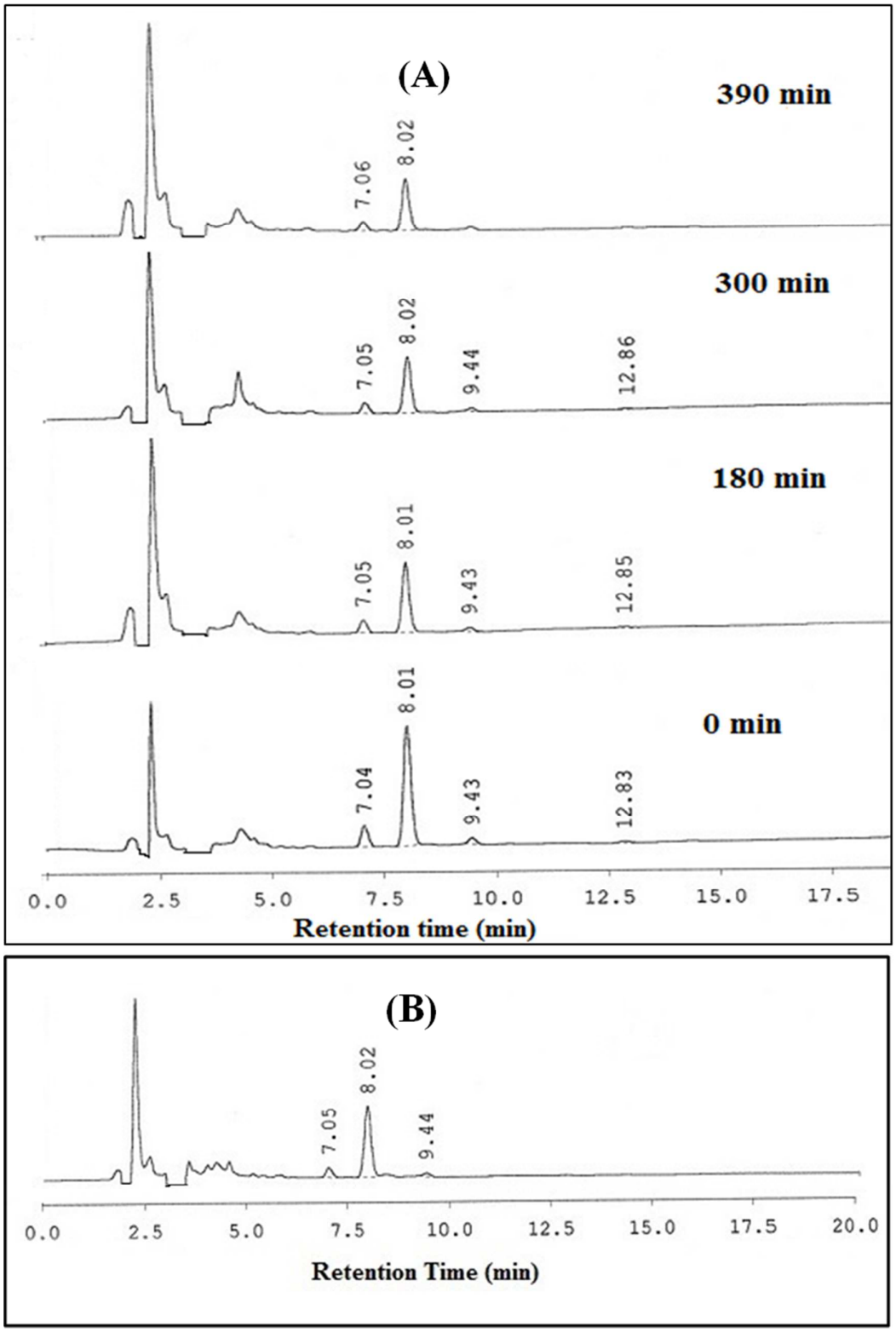

Fig. 8 High Performance Liquid Chromatograms of CR (A) obtained at different irradiation times over TiO_2 and (B) over NiST at 240 min

[Reaction conditions: [CR]= 2.5×10^{-4} M, V=100 mL and Catalyst weight- (0.25g)]

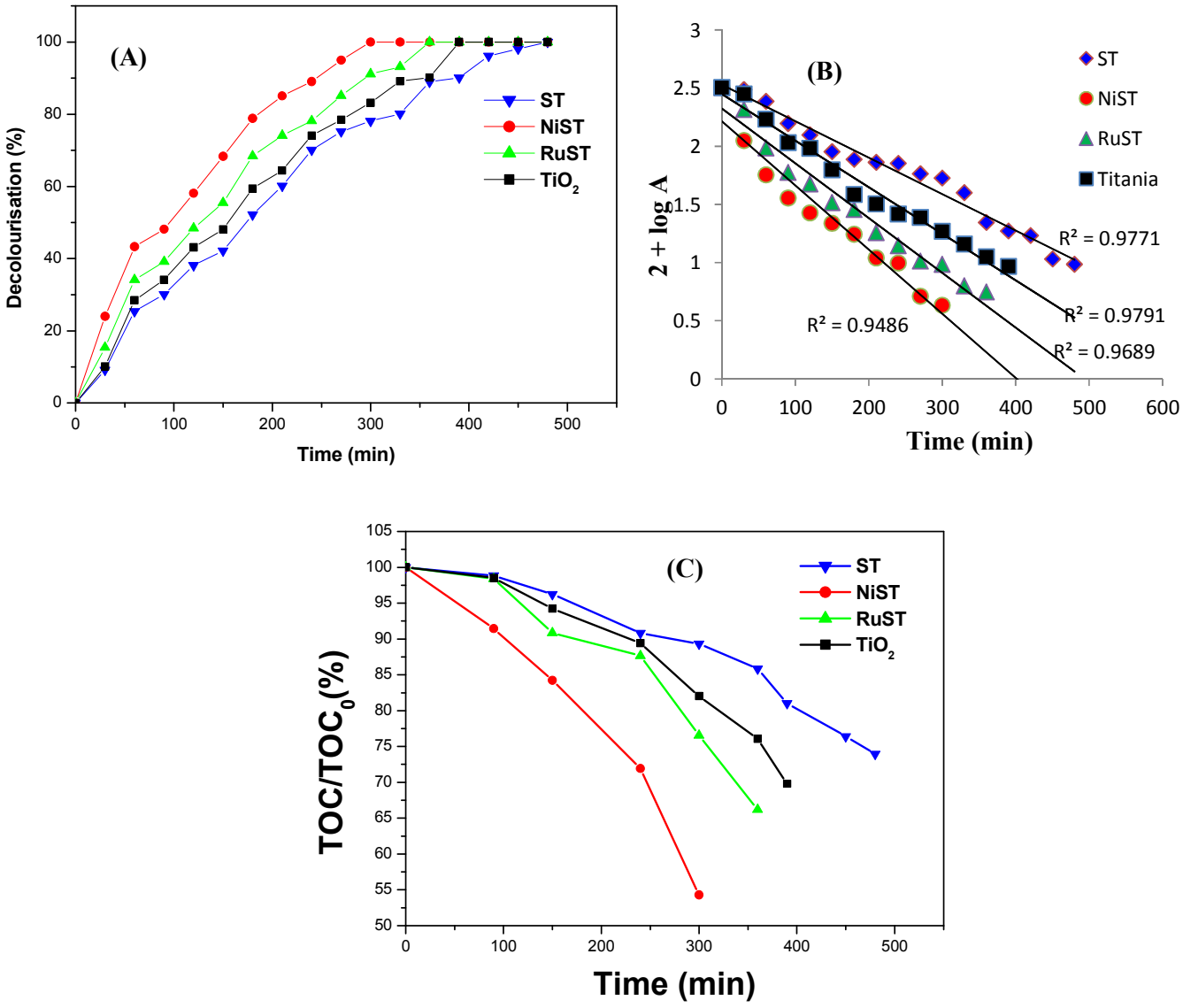

Fig. 9 (A) & (B) Decolourisation profile and kinetics of decolourisation of CR **(C)** Degradation of CR

[Reaction conditions: [CR]= 2.5×10^{-4} M, V=100 mL, Catalyst weight- (0.25g) , pH- natural pH]

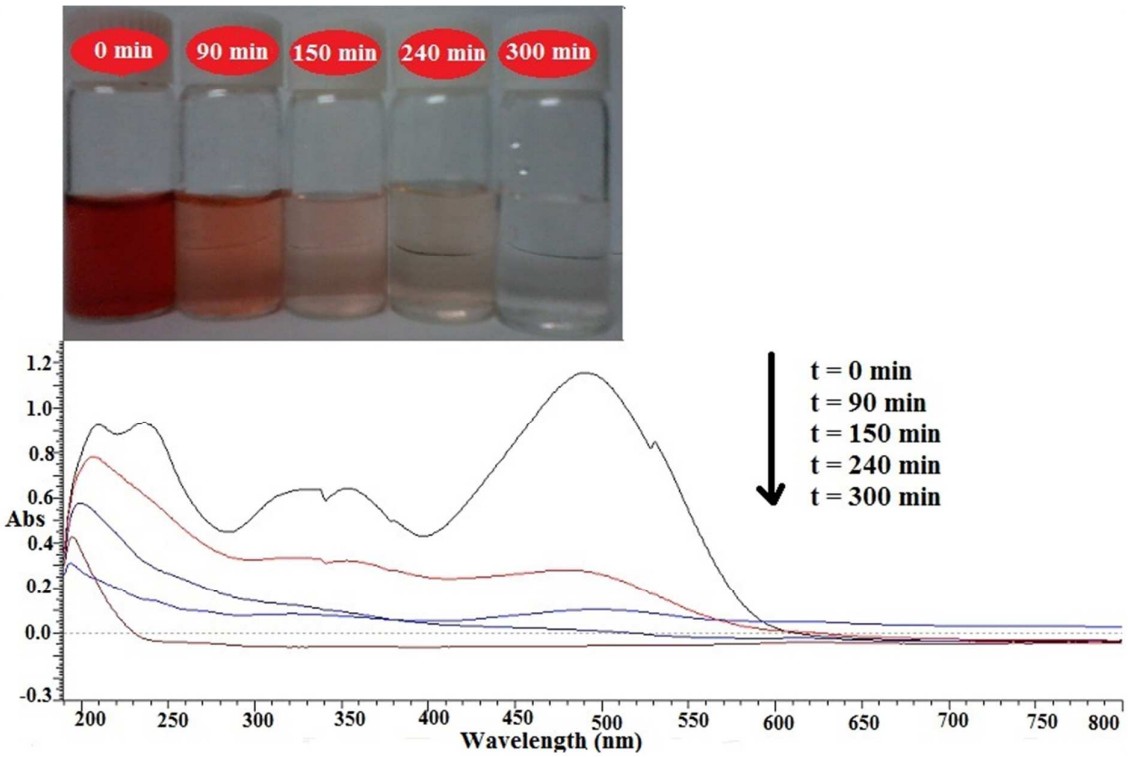

Fig. 10 UV- Vis spectral profiles of CR at various reaction times

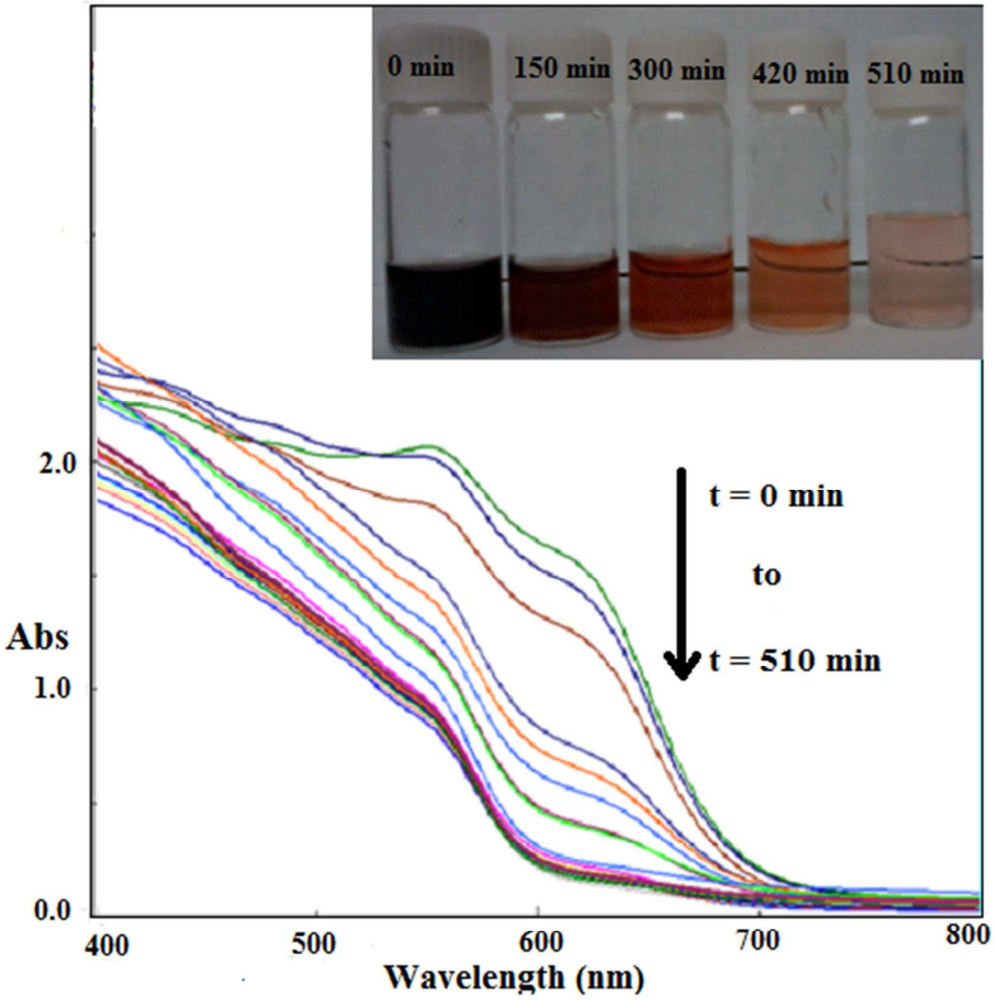

Fig. 11 UV-Vis spectra showing the photocatalytic decolourisation of textile effluent at various reaction times over NiST

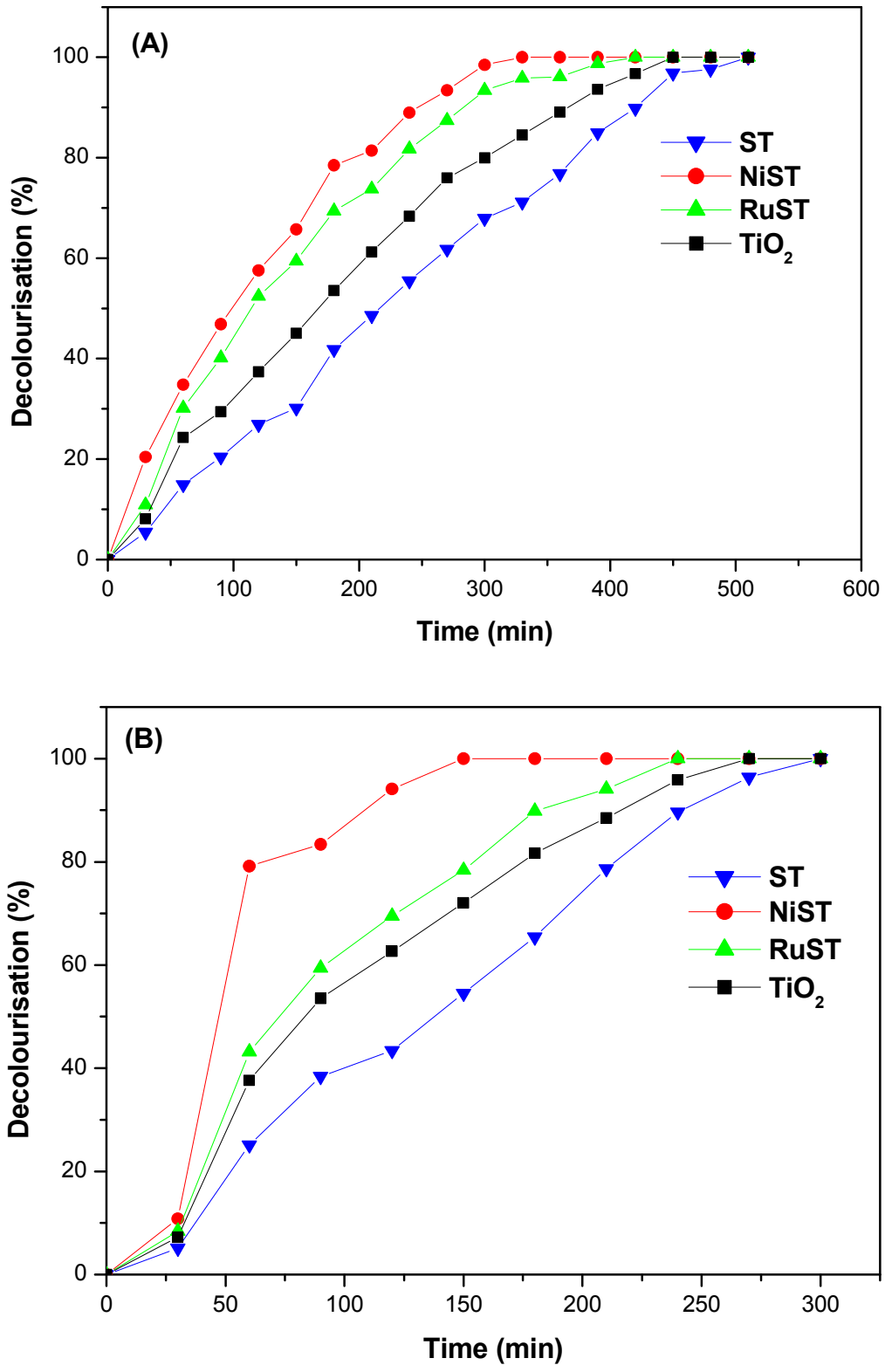

Fig. 12 (A) Decolourisation of CR under sunlight irradiation and (B) under visible irradiation

[Reaction conditions: [CR]= 2.5×10^{-4} M for sunlight studies, [CR]= 2.5×10^{-5} M for visible studies, V= 100 mL, Catalyst weight -0.25g, pH- natural pH]